



Low temperature superparamagnetic nanocomposites obtained by $\text{Fe}(\text{acac})_3$ - SiO_2 -PVA hybrid xerogel thermolysis[☆]

Catalin Ianasi¹, Otilia Costisor^{1,*}, Ana-Maria Putz¹, Radu Lazau², Adina Negrea², Daniel Niznansky³, Liviu Sacarescu⁴, Cecilia Savii^{1,*}

¹Institute of Chemistry Timisoara of Romanian Academy, Bv. Mihai Viteazul 24, 300223 Timisoara, Romania

²Faculty of Chemistry and Environmental Engineering, Polytechnic University Timisoara, Bv. Vasile Parvan 6, 300223, Timisoara, Romania

³Department of Inorganic Chemistry, Faculty of Science, Charles University in Prague Street: Hlavova 2030/8, 128 43 Prague 2, Czech Republic

⁴Institute of Macromolecular Chemistry “Petru Poni”, Aleea Grigore Ghica Voda 41A, 700487 Iasi, Romania

Received 19 October 2016; Received in revised form 18 November 2016; Accepted 9 December 2016

Abstract

Fe(acac)₃/silica/PVA hybrid xerogel nanocomposite was obtained by one pot acid catalysed sol-gel synthesis using the homogeneous mixture of iron(III) acetylacetonate (Fe(acac)₃), tetraethylorthosilicate (TEOS), and polyvinyl alcohol (PVA). Nominal composition ratio of iron oxide/silica was 15/85 (weight percent). Nitric acid was used as catalyst. Another sample of Fe(acac)₃/silica xerogel without PVA addition was prepared in the similar processing conditions. Based on thermal analysis studies, the thermal behaviour of both xerogel samples was unveiled and it allowed choosing the optimal calcination temperatures in order to obtain iron oxide silica magnetic nanocomposite samples. The two xerogel (with and without PVA) samples were thermally treated, in air, at 220, 260 and 300 °C and characterized by different techniques. XRD investigations revealed phase composition evolution with calcination temperature, from cubic spinel phase (maghemite) to hexagonal stable hematite containing nanocomposite of 10–20 nm average crystallite size. These findings were confirmed by Mössbauer spectroscopy. Up to 300 °C, the surface area and total pores volume increased with temperature for all samples. By calcination at the same temperature, the hybrid xerogel containing PVA resulted in significantly higher magnetization and free volume values in comparison with the sample without PVA.

Keywords: superparamagnetic nanocomposites, maghemite, silica, $\text{Fe}(\text{acac})_3$, polyvinyl alcohol, sol-gel

I. Introduction

During last decade, the nanotechnologies reached the great progress in preparation and characterization of magnetic nanostructured materials with tailored properties, that can be used for different applications, such as drug/gene delivery [1–6]; bioseparation [7,8], magnetic resonance imaging, [8–11] hyperthermia [12] but also as the catalysts in chemical synthesis [13]. Certain combination among different material properties, such as magnetization and high specific surface area and porosity,

low particle size etc., are essentials for different targeted applications. It is well known that the same material can exhibit different behaviour, for example magnetic properties, depending on its particle size [14]. Diverse approaches can be used in order to obtain desired properties of nanostructured materials [15–19], among which sol-gel method [20–22] could be a suitable one. Using the sol-gel route one can easily tailor and control the material morphology and texture [23].

The hybrid materials that basically were obtained by combining organic and inorganic parts, result in improved properties, compared with each single component. In the research of hybrids, the materials having higher content of organic part than inorganic part (organic-inorganic) are mainly studied. The composi-

[☆]Dedicated to the 150th Anniversary of the Romanian Academy

*Corresponding author: tel: +40 25 649 1818,

e-mail: ceciliasavii@yahoo.com (Cecilia Savii)

e-mail: o_costisor@acad-icht.tm.edu.ro (Otilia Costisor)

tions having greater inorganic versus organic amount (inorganic-organic hybrids) are rarely studied. The inorganic-organic hybrid material itself may show interesting and useful physical properties [24–27]. It also may serve as a precursor to a porous material in which pore diameter and volume may be controlled by the physical volume and the chemical character of incorporated organic phase [28–31]. To our best knowledge, the problem of physically incorporated organic phase influence on textural properties is scarcely described in the available literature. In other words, the organic polymer (polyvinyl alcohol, PVA) is usually used to be a part of synthesized hybrid material but eventually it is removed by thermal treatment. However, we presume that beside the porogen and/or surfactant roles [32] in the hybrid system, PVA can also be reducing agent [33,34] during its thermal decomposition and even after its removal, due to memory effect [35,36]. The resulting materials can be markedly mesmerized by previous PVA presence.

The present paper reports, in a first step, the synthesis and characterization of a hybrid material where the organic polymer (PVA) is incorporated in the inorganic silica xerogel forming the matrix for iron oxide precursor (iron (III) acetylacetonate) and the whole material fall into category of hybrid nanocomposites. Moreover, in the second step, the organic part was decomposed and released by heat treatment [37]. The main objective of the paper was to find the suitable preparation parameters in order to obtain superparamagnetic iron oxide-silica porous nanocomposites, maximizing the saturation magnetization at the lowest possible temperature of calcination. Further aim of the present work was to study and understand the influence of PVA, even in small amount, mainly on the magnetic properties by comparison with the system prepared without PVA. High saturation magnetization of superparamagnetic material combined with high total pore volume might define a suitable candidate to be used as inorganic magnetically responsive drug delivery vehicle having high loading capacity [38], as well as MRI contrast agent [39].

II. Material and methods

2.1. Materials

All chemicals were commercially available: polyvinyl alcohol 72000 (PVA, degree of hydroxylation >98%, Merck); tetraethyl ortho-silicate (TEOS, 98%, for synthesis, Merck); Fe(acac)₃ (99%, for synthesis, Merck); methanol (99%, for analysis, Chimopar); nitric acid (HNO₃), (65%, for analysis, Merck), distilled water.

2.2. Synthesis

Fe(acac)₃/silica/PVA hybrid xerogel nanocomposite was synthesized by acid catalysed sol-gel route using the reactant mole ratio TEOS : H₂O : PVA : Fe(acac)₃

: CH₃OH : HNO₃ = 1 : 10 : 1.2×10⁻⁵ : 0.14 : 18 : 0.01. Three precursor solutions were previously prepared. PVA solution was prepared by dissolving 2.04 g of PVA in 90 ml of distilled water at 85 °C, under stirring (2 hours). The obtained solution was cooled down to room temperature and was put into a 100 ml flask. Methanolic solution of Fe(acac)₃ was prepared by dissolving 5.41 g of Fe(acac)₃ in 80 ml of methanol at 50 °C under stirring for 15 minutes. Catalyst solution (pH~1.5) was prepared by diluting of 0.07 g of 65% HNO₃ with 15.14 g of distilled water.

15.21 g of the catalyst solution was added to 23.74 g TEOS under stirring (30 minutes) until the resulted sol became transparent. 5 g of the 2%-PVA solution was then added and held under continuous stirring for another 15 minutes. The previously prepared methanolic solution of Fe(acac)₃ was subsequently added to SiO₂-PVA sol and stirred for another 15 minutes at 55 °C. The Fe(acac)₃/silica/PVA system was covered and left at room temperature to form a gel. The gelation occurred after 4 days. The obtained Fe(acac)₃/silica/PVA hybrid xerogel was labelled as a function of molecular mass of used organic polymer N-72 ($M_{wPVA} = 72000$). Another Fe(acac)₃/silica nanocomposite sample, labelled N-0, was prepared under the same conditions without adding PVA.

The two xerogel samples were subsequently thermally treated at three different temperatures: 220, 260 and 300 °C. The choice of the heat treatment temperatures was based on thermogravimetric analysis. The obtained samples were labelled by adding the heat treatment temperature to the xerogel sample name as follows: N-72-220, N-72-260, and N-72-300; N-0-220, N-0-260 and N-0-300.

2.3. Characterization methods

Thermogravimetric analysis was carried out between 25 and 800 °C in air flow at 5 °C/min heating rate, using an 851-LF 1100-Mettler Toledo apparatus. The phase composition of the powders was determined by X-ray diffraction, using a Rigaku Ultima IV instrument. The X-ray diffraction patterns were recorded using glass support and monochromatic CuK α radiation. The diffraction patterns were measured in 2 θ range of 25–65°. Crystallite size was calculated from diffraction lines broadening by using the Scherrer equation. Morphology of the samples was characterized by using a High-Tech HT7700 Transmission Electron Microscope (Hitachi). The samples were analysed in high contrast mode at 100 kV accelerating voltage using copper grids (Ted Pella). FTIR spectra were recorded on samples, pressed into pellets, prepared with KBr, using a JASCO FT/IR-4200 apparatus. Textural properties of nanocomposites were analysed using nitrogen adsorption/desorption measurements at liquid nitrogen temperature (77 K) with a Quantachrome Nova 1200e apparatus. Before measurements the samples were degassed in vacuum at room temperature for 4 hours. The mag-

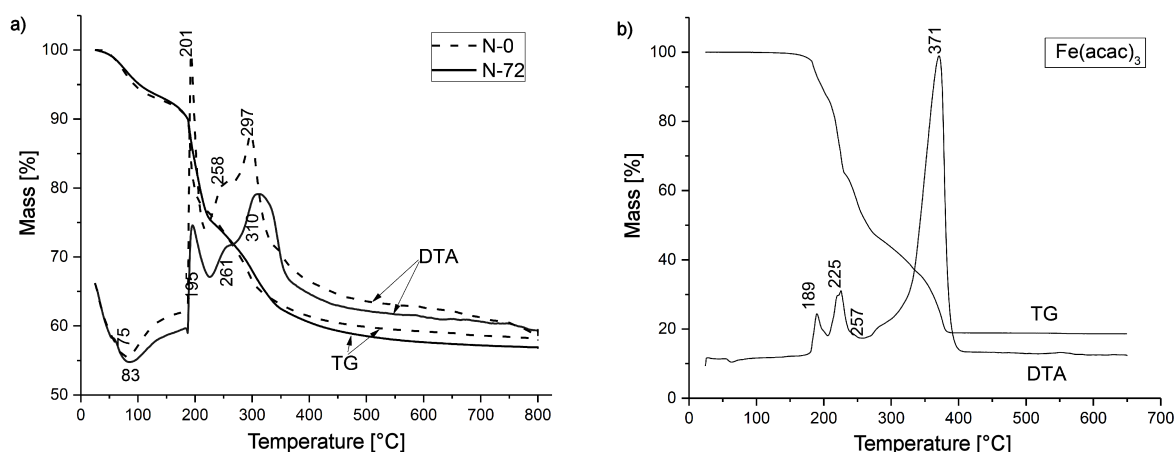


Figure 1. TGA and DTA of: a) samples with PVA (N-72) and without PVA (N-0) and b) pure $\text{Fe}(\text{acac})_3$

netic properties were investigated in AC (50Hz) field of 5 kOe amplitude by means of a home-made induction magnetometer [40]; the apparatus was calibrated for specific magnetization using a Ni powder reference (99.8% purity, 30 μm mean grain diameter, Sigma-Aldrich). The magnetic hysteresis loops were recorded to a PC using a 16-bit resolution data acquisition card DT-9816A (Data Translation), and the specific magnetization at technical saturation was estimated from extrapolation to the field of 5 kOe with a superposition of Langevin functions.

III. Results and discussion

3.1. Thermal analysis

Thermogravimetric (TGA) and differential thermal analysis (DTA) studies were carried out in order to determine the heat treatment temperatures based on gradual degradation of organic part and release of its decomposition products from matrix. The thermal analysis was carried out for the nanocomposite xerogel ($\text{Fe}(\text{acac})_3/\text{silica}$) samples without and with PVA) denoted as N-0 and N-72, respectively, and for pure $\text{Fe}(\text{acac})_3$, and the results are presented in Fig. 1 and Table 1.

Four distinct transformation steps were observed in the case of both nanocomposite xerogel samples. The decomposition of both samples was completed at 400 $^{\circ}\text{C}$ and the total weight loss was: 42.08 wt.% for N-0 and 43.15 wt.% for N-72. This small difference might be due to decomposition of PVA and higher ratio between organic and inorganic components in the sample N-72 with PVA than in the sample N-0 without PVA. In the first step ranging from 25 to 125 $^{\circ}\text{C}$, we can observe endothermic effect related to the loss of the small molecules such as residual water and other solvents inside the xerogel samples [41,42]. The second step in the range of 125–225 $^{\circ}\text{C}$ corresponds to the loss of structural water [43] and removal of parts of organics [44] and mainly to the partial decomposition of $\text{Fe}(\text{acac})_3$ [45,46]. In the third temperature interval, 225–275 $^{\circ}\text{C}$ the mass loss and exothermic effects were assigned to the condensation [47] and dehydroxylation of silica matrix, removal of organics [44] and PVA polymer chains cleavage [48]. Also, according to Pal *et al.* [46], this exothermic effect is due to the elimination of acetylacetonate group from the metal-organic compound and transformation into maghemite ($\gamma\text{-Fe}_2\text{O}_3$). The last thermal effect is assigned to the removal of organic residues and carbon resulting from anaerobic decomposition of

Table 1. TGA and DTA results

| Sample | Temperature domain [°C] | Weight loss [wt.%] | Thermal effect | T_{max} [°C] |
|----------------------------|-------------------------|--------------------|----------------|----------------|
| N-0 | 25–125 | 6.75 | endothermic | 75 |
| N-72 | | 6.21 | endothermic | 83 |
| $\text{Fe}(\text{acac})_3$ | | - | - | - |
| N-0 | 125–225 | 16.94 | exothermic | 201 |
| N-72 | | 18.28 | exothermic | 195 |
| $\text{Fe}(\text{acac})_3$ | | 36.36 | exothermic | 189; 225 |
| N-0 | 225–275 | 5.84 | exothermic | 258 |
| N-72 | | 4.47 | exothermic | 261 |
| $\text{Fe}(\text{acac})_3$ | | 18.44 | endothermic | 257 |
| N-0 | 275–800 | 12.55 | exothermic | 297 |
| N-72 | | 14.19 | exothermic | 310 |
| $\text{Fe}(\text{acac})_3$ | | 26.94 | exothermic | 371 |

organic compounds [44] and further condensation of OH groups in the silica matrix [42,49]. In this temperature range, the C–C bonds of the polymer are cleaved [48] and also some remains of $\text{Fe}(\text{acac})_3$ can be decomposed into $\gamma\text{-Fe}_2\text{O}_3$. The hematite ($\alpha\text{-Fe}_2\text{O}_3$), which is the only stable phase of iron oxide, starts to appear.

For all samples, it was observed that the main weight loss occurs in the temperature interval of 125–225 °C, where $\text{Fe}(\text{acac})_3$ itself decomposes, showing the maximum weight loss [43].

3.2. X-ray diffraction

The X-ray diffractograms of both series of nanocomposites, prepared by thermal treatment of inorganic and hybrid xerogels at 260 and 300 °C, are shown in Fig. 2. The X-ray diffraction patterns of both samples, thermally treated at 220 and 260 °C are very similar (for this reason only 260 °C heat treated samples are presented) and manifest characteristic lines of a face-centred cubic spinel structure [50]. For the samples treated at 300 °C, we can observe additional diffraction peaks; the most intense one is situated at $2\theta \sim 33^\circ$, which corresponds to hematite [51]. It means that some part of the iron oxide was already transformed into hematite which is only stable phase of Fe_2O_3 . By using XRD technique, it is not possible to distinguish between magnetite and maghemite, because their diffraction patterns are very similar. This problem was solved by Mössbauer spectroscopy which is discussed later.

Iron oxide diffraction lines in XRD pattern of the sample heat treated 220 °C (data not shown) are very broad corresponding to very small particles. With the increase in temperature, we can follow the decrease of the peak widths. This line sharpening corresponds to both the increased crystallinity and the crystallite growth. Crystallite sizes were calculated from diffraction lines broadening by using the Scherrer equation:

$$D_{(hkl)} = \frac{K\lambda}{b_{(hkl)} \cos \theta} \quad (1)$$

where D is the average crystallite size (diameter) and

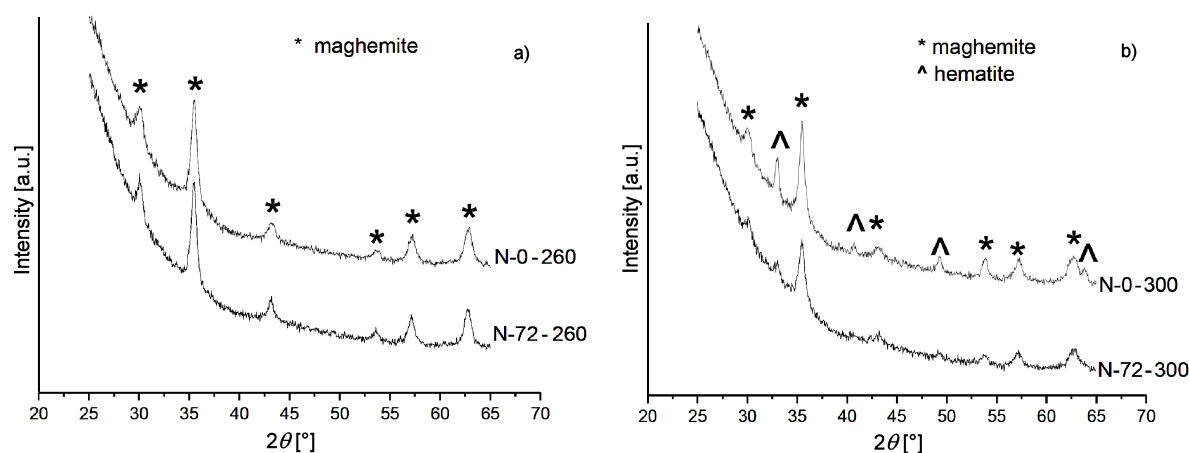


Figure 2. XRD patterns of both series thermally treated at: a) 260 °C (N-0-260 and N-72-260 samples) and b) 300 °C (N-0-300 and N-72-300 samples)

b is the structural broadening of diffraction peaks. The calculated crystallite sizes for all samples are presented in Table 2.

The crystallite sizes for all heat treated samples are similar (about 15 nm) with the exception of the sample containing PVA heat treated at 300 °C. This is in agreement with the fact that the particle growth does not occur in this temperature range.

Table 2. Phase composition and average crystallite size ($D_{(hkl)}$) of xerogels heated at 220, 260 and 300 °C

| Sample | Phase composition | $D_{(hkl)}$ [nm] |
|----------|-------------------------|------------------|
| N-0-220 | maghemite | 16 |
| N-72-220 | maghemite | 16 |
| N-0-260 | maghemite | 13 |
| N-72-260 | maghemite | 16 |
| N-0-300 | maghemite + hematite | 15 25 |
| N-72-300 | maghemite + hematite | 21 20 |

3.3. Fourier transformation infrared spectroscopy

The FTIR spectra of the xerogel samples N-0 and N-72 (without and with PVA) are presented in Fig. 3a. The xerogel samples composition was quite complex. Generally, it can be assumed the presence of silica developed network, starting from silica alkoxide by hydrolysis and condensation, that encompassing iron acetylacetonate solution, polyvinyl alcohol and solvents. The band at 434 cm^{-1} , observed in both xerogel spectra, was assigned to Si–OC₂H₅ bond and/or Si–O–C deformation vibrations, and Fe–O bond, probably coming from the precursors, (TEOS) traces and Fe acetylacetonate, respectively [52–55]. Specific IR features at 1634 cm^{-1} (O–H), 1277 cm^{-1} (C–CH₃ and C=C), 1216 cm^{-1} (CH₃), 1138 cm^{-1} (C–H) and 676 cm^{-1} (O–H) were attributed to the acetylacetonate organic part and in the same time to PVA [(-CH₂-CHOH)-]_n and alcohols (CH₃OH and C₂H₅OH).

By increasing the calcination temperature the de-

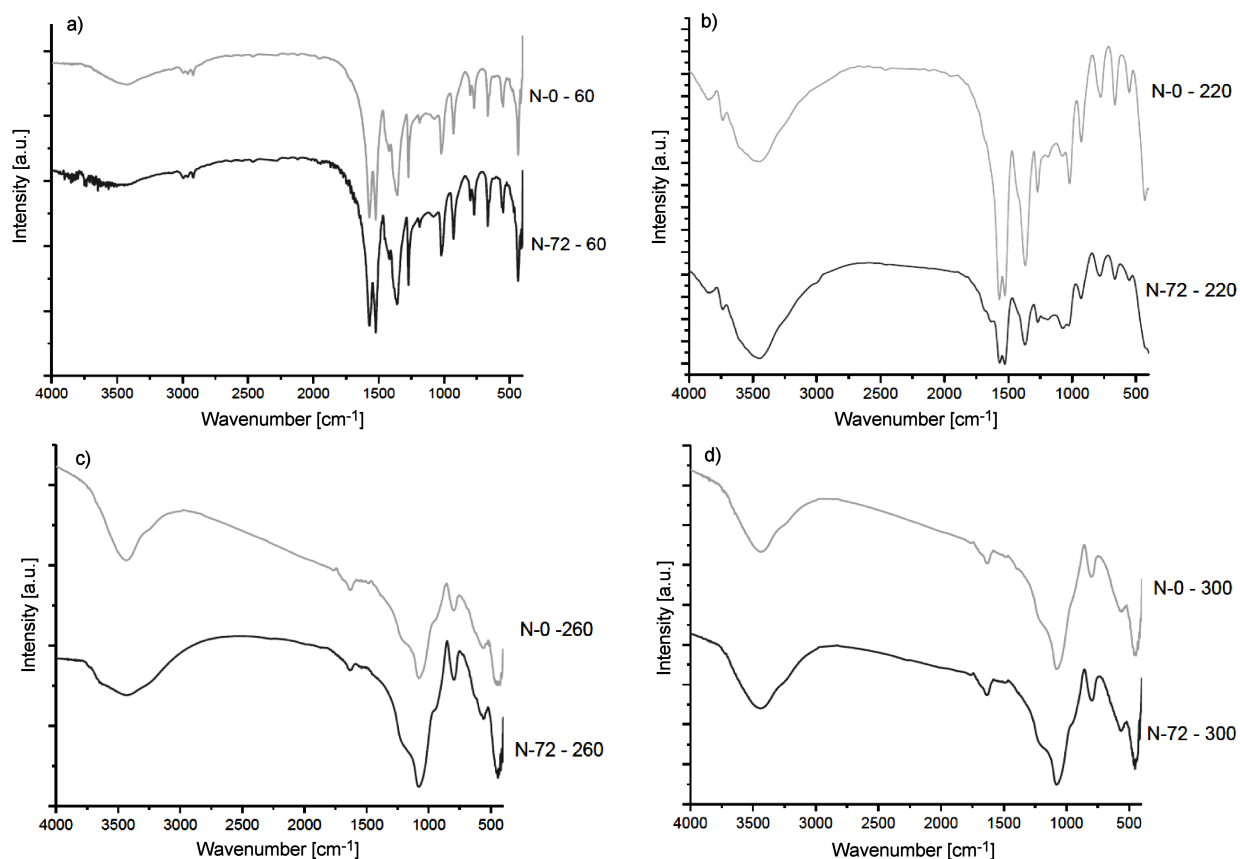


Figure 3. FTIR spectra of all nanocomposites obtained after thermal treatment at a) 60 °C, b) 220 °C, c) 260 °C and d) 300 °C

crease, disappearance or new developments in the IR spectra (Figs. 3b-d) were observed. Because of superimposed IR signals, the precise interpretation of spectra was difficult. However, some observations of IR band evolution can offer certain information concerning thermal behaviour of the two xerogel samples. For example, we can observe an increase of the 1075 cm^{-1} band (assigned to Si–O–Si and Si–O stretching vibrations) with temperature, and simultaneous decrease of 952 cm^{-1} band intensity (assigned to Si–OH) which indicates that further condensation process was running during thermal treatment. At each increase in tempera-

ture, the 550 cm^{-1} and 440 cm^{-1} band intensities, mainly assigned to Fe–O bonds, are increasing [56]. Apparently, at the final calcination temperature (300 °C) the largest part of the organic compounds is decomposed and the transition process from maghemite to hematite has begun. These results are consistent with TG-DTA and XRD data.

3.4. Transmission electron microscopy

The TEM images of the sample N-0 (without PVA) heated at different temperatures are presented in Fig. 4. The average size of maghemite nanoparticles in the

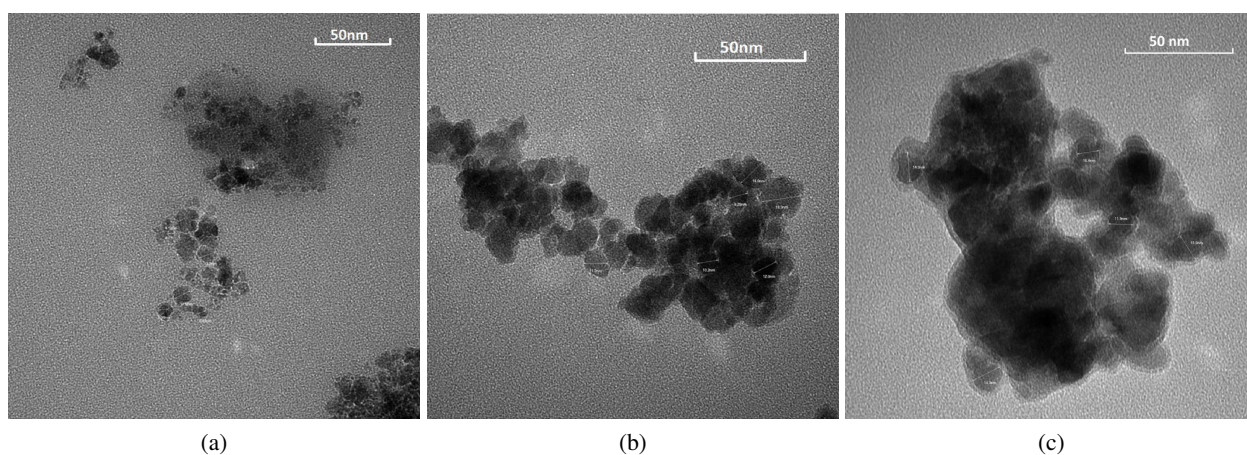


Figure 4. TEM images of: a) N-0-220, b) N-0-260 and c) N-0-300 samples

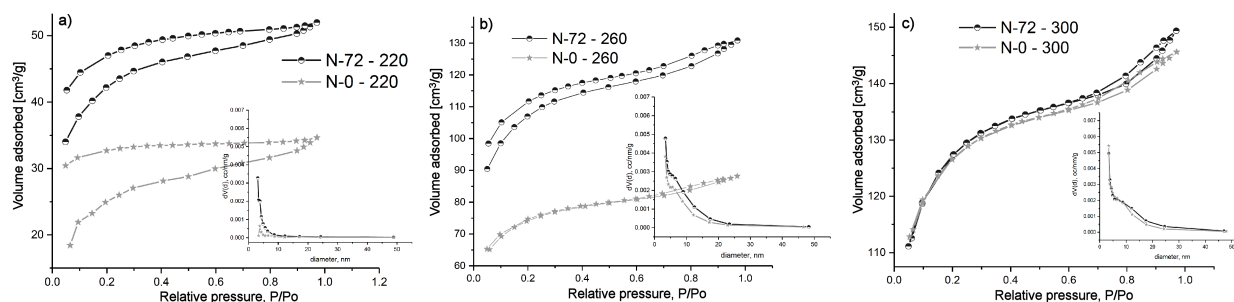


Figure 5. Adsorption-desorption isotherms and pore size distribution (inset) obtained after calcination the nanocomposites at a) 220 °C, b) 260 °C and c) 300 °C

sample thermally treated at 260 °C is about 15 nm (Fig. 4b). However, after the thermal treatment at 300 °C (Fig. 4c) the dimensions of the particles are not changed much but they tend to agglomerate.

3.5. Nitrogen adsorption-desorption method

Further information about porous systems were obtained using adsorption-desorption measurements. The adsorption-desorption isotherms and pore size distribution (inset) of the samples obtained after the thermal treatment are presented in Fig. 5.

According to IUPAC classification, all obtained adsorption-desorption isotherms are corresponding to type IV which is generally associated with capillary condensation in mesopores [57]. However, the hysteresis loops of H4 type are indication that along with mesopores, micropores are also present [58]. Type H4 loop is associated with narrow slit or plate like pores [57]. The samples calcined at 220 °C show an unusual type of open isotherm, which might be due to the presence of various residual organic groups on the surface and increased microporosity [59]. The most organics were removed from the material surface with the further increase of the calcination temperature up to 300 °C, and consequently the isotherms were closed (Fig. 5c). The pore size distribution shows the pore diameter of ~3 nm which is characteristic for all samples (Table 3).

Significant differences concerning texture properties between two kinds of samples were not observed at 300 °C. It has to be noted that the nanocomposite samples, obtained at 260 °C, having the unique crystalline phase (maghemite with superparamagnetic behaviour), are quite different regarding the texture properties. The most suitable sample to be further used in biomedical applications was N-72-260 (derived from PVA hybrid

xerogel) [39] with increased surface area and pore volume 40% higher than the sample prepared without PVA.

3.6. Mössbauer spectroscopy

The Mössbauer spectroscopy (MS) helps us to precise spinel crystalline phase assignment, based on iron cations speciation (Fe^0 , Fe^{2+} and Fe^{3+}) and distribution in the network sites (octahedral and tetrahedral). At the same time, we can also obtain the information about magnetic ordering in the samples. The samples which show sextet are magnetically ordered, while the samples that show doublet are magnetically disordered. The amount of phases was determined from the area of Mossbauer subspectra taking into account the Mossbauer recoilless factor to be 1 for all contributions.

The MS measurements of the calcined nanocomposite samples, based on N-0 xerogel are presented in Fig. 6 and Table 4. Amorphous and magnetically disordered sample was represented by the doublet (subspectrum 1) and ordered phase maghemite was represented by sextets (subspectra 2 and 3). In the case of maghemite, the isomer shift in the range of 0.2 to 0.4 mm/s indicates that only Fe^{3+} was present. The sextets show the non-symmetric aspect of peaks having slower shift of ΔE_Q towards 0 mm/s. This is typical behaviour of the MS of $\gamma\text{-Fe}_2\text{O}_3$ where vacancies in octahedral positions cause the distribution of hyperfine field. Subspectrum 4, observed only in the case of the magnetic nanocomposite sample obtained at 300 °C, was attributed to the hematite phase. The intensity of doublet progressively decreases with the increase in temperature and at the same time, the intensity of sextet increases. That means, by increasing the calcination temperature (from 220 to 300 °C) significant growth of magnetically ordered phase amount was observed, maghemite (from 50 to

Table 3. Texture characteristics for xerogel samples heat treated at 220, 260 and 300 °C

| Sample | BET, surface area [m ² /g] | BJH [nm] | TPV [cm ³ /g] | Alpha-S, micropore volume, [cm ³ /g] |
|----------|--|-------------|-----------------------------|--|
| N-0-220 | 84 | 3.18 | 0.05 | 0.02 |
| N-72-220 | 137 | 3.08 | 0.08 | 0.05 |
| N-0-260 | 232 | 3.40 | 0.13 | 0.09 |
| N-72-260 | 341 | 3.41 | 0.20 | 0.13 |
| N-0-300 | 392 | 3.38 | 0.22 | 0.17 |
| N-72-300 | 398 | 3.43 | 0.23 | 0.17 |

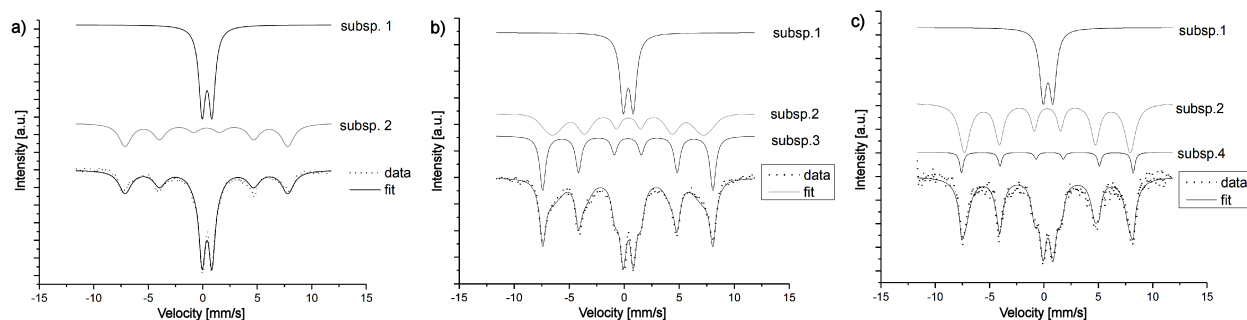


Figure 6. Mössbauer spectra of a) N-0-220, b) N-0-260 and c) N-0-300 samples

65%) and hematite (from 0 to 6%). The maghemite was developed on the expense of the amorphous, non-ordered phase, which decreased from 50 to 29%. It was not clear if the hematite developed from amorphous phase crystallization or in maghemite-hematite transition process, because both crystalline phases amounts are increasing.

XRD results practically indicate that there are no significant differences between N-0-260 and N-0-300 samples. This can be explained by partial crystallization and crystalline network healing by defect removals in the iron oxide particles which occurs without simultaneous particle growth. We can follow the same tendency in the series generated by thermolysis of N-72 xerogel, subsequently presented in Fig. 7 and Table 5.

The subspectrum 1 (doublet) corresponds to iron oxide magnetically non-ordered phase. The subspectra 2 and 3, in the case of N-72-260 sample, and (2+3) unique subspectrum of N-72-300 sample, correspond to magnetically ordered maghemite phase. The sample heat treated at 300 °C contains 9% of hematite phase, also magnetically ordered, as the subspectrum 4 (N-72-300 MS) showed. Certain difference among specific MS features observed in the two cases (without and with PVA) has to be noted. In the case of hybrid xerogels with PVA derived nanocomposites, the growth mechanism of the magnetically ordered phases seems to be altered with calcination temperature compared to the case of silica xerogel derived nanocomposites without PVA. The increased temperature of thermal treatment from 260 to 300 °C resulted in simultaneous maghemite amount diminishing from 73 to 63%, and hematite phase growing from 0 to 9%, while the amorphous phase con-

tent (27–28%) remained practically the same. As it follows, in the case of hybrid xerogel derived nanocomposite, N-72-300, without doubt the hematite originates from maghemite-hematite transition process. The Quadrupole splitting value evolution, specifically the faster shift of ΔE_Q towards 0 mm/s, put in evidence a more symmetric aspect of the sextet's peaks. Even more, for the sample heat treated at 300 °C, N-72-300, MS showed $\Delta E_Q = 0$ for maghemite phase representative unique subspectrum. As previously shown, this is typical behaviour of the MS of $\gamma\text{-Fe}_2\text{O}_3$ related to vacancies in octahedral positions that influence the distribution of hyperfine field.

These results are in agreement with XRD, where we can observe the diffraction peaks of maghemite and hematite. When we compare MS of two samples (the xerogels without and with PVA heat treated at 260 and 300 °C), we can see that MS of PVA hybrid derived samples manifest higher surface area of sextets in comparison with doublet so we can conclude that the use of PVA leads to either larger particles or more perfect crystal structure or both.

3.7. Magnetization measurements

The dependence of magnetization on applied magnetic field was measured at room temperature. The magnetization curves for all heat treated samples are shown in Fig. 8. In addition, the values of the coercivity (H_c), the remanence (σ_r), and the saturation magnetizations (σ_{sat}) are summarized in Table 6.

Both σ_{sat} and H_c values increase with the calcination temperature between 220 °C and 260 °C, while there is practically insignificant evolution between 260 °C and

Table 4. The Mössbauer parameters for N-0-220, N-0-260 and N-0-300 samples

| Sample | Isomer shift [mm/s] | Quadrupole splitting ΔE_Q [mm/s] | Hiperfine field B_{Hf} [T] | Relative area [%] |
|------------------|------------------------|---|---------------------------------|----------------------|
| N-0-220 Subsp. 1 | 0.37 | 0.86 | N/A | 50 |
| N-0-220 Subsp. 2 | 0.28 | -0.28 | 44.21 | 50 |
| N-0-260 Subsp. 1 | 0.36 | 0.92 | N/A | 41 |
| N-0-260 Subsp. 2 | 0.30 | -0.11 | 43.00 | 10 |
| N-0-260 Subsp. 3 | 0.32 | -0.01 | 47.52 | 49 |
| N-0-300 Subsp. 1 | 0.36 | 0.89 | N/A | 29 |
| N-0-300 Subsp. 2 | 0.31 | 0.03 | 48.19 | 25 |
| N-0-300 Subsp. 3 | 0.36 | -0.04 | 43.51 | 40 |
| N-0-300 Subsp. 4 | 0.37 | -0.2 | 49.00 | 6 |

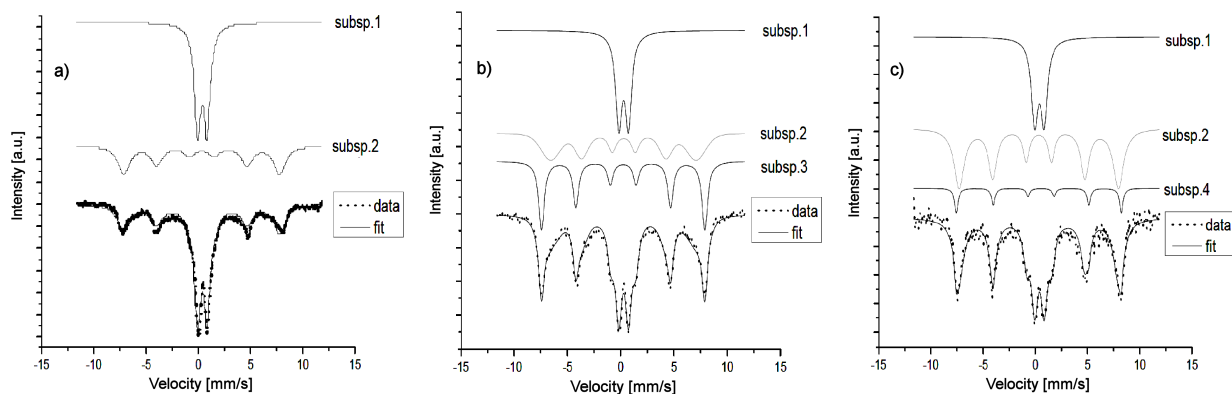


Figure 7. Mössbauer spectra of samples: a) N-72-220, b) N-72-260 and c) N-72-300

Table 5. The Mössbauer parameters for samples N-72-220, N-72-260 and N-72-300

| Sample | Isomer shift [mm/s] | Quadrupole splitting ΔE_Q [mm/s] | Hiperfine field B_{Hf} [T] | Relative area [%] |
|--------------------|---------------------|--|------------------------------|-------------------|
| N-72-220 Subsp. 1 | 0.39 | 0.91 | N/A | 49 |
| N-72-220 Subsp. 2 | 0.34 | -0.02 | 46.35 | 51 |
| N-72-260 Subsp. 1 | 0.37 | 0.91 | N/A | 27 |
| N-72-260 Subsp. 2 | 0.36 | -0.04 | 42.85 | 37 |
| N-72-260 Subsp. 3 | 0.32 | -0.002 | 48.07 | 36 |
| N-0-300 Subsp. 1 | 0.36 | 0.90 | N/A | 28 |
| N-0-300 Subsp. 2+3 | 0.31 | 0 | 47.37 | 63 |
| N-0-300 Subsp. 4 | 0.42 | -0.21 | 49.06 | 9 |

300 °C in the case of samples without PVA. The explanation of this evolution is analogous to those used in the case of MS interpretation. Specifically, when we increase calcination temperature from 260 °C to 300 °C, the partial crystallization and defect removal in the iron oxide particles occurs, without simultaneous particle growth. The same tendency can be followed in the case of magnetic nanocomposite samples based on PVA con-

taining hybrid xerogels. But once again when we compare σ_{sat} and H_c values of two samples (with and without PVA) heat treated at 300 °C, we can see that the σ_{sat} and H_c of PVA containing samples manifest greater values in comparison with sample without PVA. The N-72-260 nanocomposite sample exhibits saturation magnetization value of 43.6 mu/g, 1.5 times higher than M_s value of N-0-260 magnetic nanocomposite sample (derived from silica xerogel without PVA). That means that during thermal treatment, including ferric precursor thermolysis, the organic polymer (PVA) has a significant positive effect on the magnetization intensity and magnetic ordering, as a reducing and directing agent [37]. It cannot be excluded the possible memory effect attributable also to the presence of polyvinyl alcohol as directing agent during sol-gel processing [43].

Small drop of σ_{sat} values for both samples with and without PVA between 260 °C and 300 °C mainly can be due to the partial transformation of γ -Fe₂O₃ into α -

Table 6. Saturation magnetization (σ_{sat}), remanent magnetization (σ_r) and coercivity (H_c) at room temperature for samples thermally treated at 220, 260 and 300 °C

| Sample | σ_{sat} [emu/g] | σ_r [emu/g] | H_c [kOe] |
|----------|------------------------|--------------------|-------------|
| N-0-220 | 1.80 | 0.09 | 0.02 |
| N-0-260 | 28.77 | 3.01 | 0.05 |
| N-0-300 | 25.46 | 2.93 | 0.06 |
| N-72-220 | 2.62 | 0.24 | 0.04 |
| N-72-260 | 43.61 | 3.81 | 0.07 |
| N-72-300 | 40.79 | 5.03 | 0.09 |

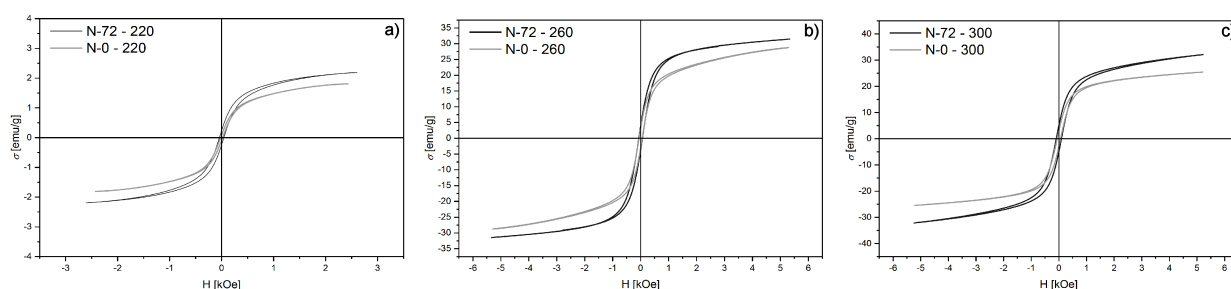


Figure 8. Room temperature magnetic hysteresis loops of heat treated samples: a) 220 °C, b) 260 °C and c) 300 °C with and without PVA

Fe₂O₃ which is very weak ferromagnet at room temperature (above Morin temperature) and practically do not contribute to the total value of σ_{sat} . On the contrary, the presence of hematite developed at the expense of maghemite has a significant magnetic dilution effect. This behaviour is consistent with the conclusions made from XRD and MS characterizations.

The comparison of magnetic behaviour of both series of samples is in good agreement with our presumptions that the use of PVA will lead to better magnetic properties of final magnetic nanocomposite.

IV. Conclusions

Two xerogel nanocomposite samples Fe(acac)₃/silica and Fe(acac)₃/silica/PVA (without and with organic polymer content, respectively) with Fe₂O₃/SiO₂ weight ratio of 15/85, were synthesized, characterized, and thermally treated. X-ray diffraction patterns showed that the maghemite was present at 260 °C as exclusive crystalline phase. At 300 °C, γ -Fe₂O₃ → α -Fe₂O₃ transition process had begun and hematite crystalline phase started to develop. Mossbauer spectroscopy measurements are consistent with XRD results. By increasing the calcination temperature to 300 °C the surface area and total pore volume were increased for both series, but the increase was faster for the material with PVA (1.5 times). These findings are consistent with presumed effects of the organic polymer (in small amount), specifically as surfactant and porogen agent. The magnetic measurement generally indicates the increase of saturation magnetization with temperature for all heat-treated samples.

Following all the results we can conclude that the use of PVA leads to a larger surface area, greater particle of more perfect crystal structure and better magnetic properties even at low temperatures. The comparison of the measured properties of both series of samples leads us to the conclusion that they are in reasonable agreement with our presumption: the use of PVA will lead to better structure, morphology and magnetic properties of resulted nanocomposites.

Acknowledgement: Authors thank the Romanian Academy and the Inter-Academic Exchange Program between Academy of Sciences of the Czech Republic and Romanian Academy. Authors thank also to Dr. Aurel Ercuta from West University of Timisoara, Romania, for magnetic measurements and fruitful discussions.

References

1. A.K. Gupta, M. Gupta, "Synthesis and surface engineering of iron oxide nanoparticles for biomedical applications", *Biomaterials*, **26** (2005) 3995–4021.
2. U. Schillinger, T. Brill, C. Rudolph, S. Huth, S. Gersting, F. Krötz, J. Hirschberger, C. Bergemann, C. Plank, "Advances in magnetofection—magnetically guided nucleic acid delivery", *J. Magn. Magn. Mater.*, **293** (2005) 501–508.
3. A.S. Lübbe, C. Bergemann, J. Brock, D.G. McClure, "Physiological aspects in magnetic drug targeting", *J. Magn. Magn. Mater.*, **194** (1999) 149–155.
4. T. Neuberger, B. Schöpf, H. Hofmann, M. Hofmann, B. Von Rechenberg, "Superparamagnetic nanoparticles for biomedical applications: Possibilities and limitations of a new drug delivery system", *J. Magn. Magn. Mater.*, **293** (2005) 483–496.
5. T.J. Yoon, J.S. Kim, B.G. Kim, K.N. Yu, M.H. Cho, J.K. Lee, "Multifunctional nanoparticles possessing a "Magnetic Motor Effect" for drug or gene delivery", *Angew. Chem. Int. Ed. Engl.*, **44** (2005) 1068–1071.
6. S. Chamorro, L. Gutiérrez, M.P. Vaquero, D. Verdoy, G. Salas, Y. Luengo, A. Brenes, F.J. Teran, "Safety assessment of chronic oral exposure to iron oxide nanoparticles", *Nanotechnology*, **26** [20] (2015) 205101.
7. I. Koh, X. Wang, B. Varughese, L. Isaacs, S.H. Ehrman, D.S. English, "Magnetic iron oxide nanoparticles for biorecognition: Evaluation of surface coverage and activity", *J. Phys. Chem. B*, **110** (2006) 1553–1558.
8. P.S. Doyle, J. Bibette, A. Bancaud, J.L. Viovy, "Self-assembled magnetic matrices for DNA separation chips", *Science*, **295** (2002) 2237.
9. O. Veiseh, C. Sun, J. Gunn, N. Kohler, P. Gabikian, D. Lee, N. Bhattarai, R. Ellenbogen, R. Sze, A. Hallahan, J. Olson, M. Zhang, "Optical and MRI multifunctional nanoprobe for targeting gliomas", *Nano. Lett.*, **5** (2005) 1003–1008.
10. C.W. Lu, Y. Hung, J.K. Hsiao, M. Yao, T.H. Chung, Y.S. Lin, S.H. Wu, S.C. Hsu, H.M. Liu, C.Y. Mou, C.S. Yang, D.M. Huang, Y.C. Chen, "Bifunctional magnetic silica nanoparticles for highly efficient human stem cell labeling", *Nano. Lett.*, **7** (2007) 149–154.
11. Y.M. Huh, Y.W. Jun, H.T. Song, S. Kim, J.S. Choi, J.H. Lee, Y. Yoon, K.S. Kim, J.S. Shin, J. S. Suh, J. Cheon, "In vivo magnetic resonance detection of cancer by using multifunctional magnetic nanocrystals", *J. Am. Chem. Soc.*, **127** (2005) 12387–12391.
12. A. Jordan, R. Scholz, P. Wust, H. Schirra, T. Schiestel, H. Schmidt, R. Felix, "Endocytosis of dextran and silan-coated magnetite nanoparticles and the effect of intracellular hyperthermia on human mammary carcinoma cells in vitro", *J. Magn. Magn. Mater.*, **194** (1999) 185–196.
13. M.C. Brasil, E.V. Benvenutti, J.R. Gregorio, A.E. Gerbase, "Iron acetylacetonate complex anchored on silica xerogel polymer", *React. Funct. Polym.*, **63** (2005) 135–141.
14. W.P. Osmond, "An interpretation of the magnetic properties of some iron-oxide powders", *Proc. Phys. Soc. London Sect. B*, **65** (1952) 2.
15. S. Rohilla, S. Kumar, P. Aghamkar, S. Sunde, A. Agarwal, "Investigations on structural and magnetic

- properties of cobalt ferrite/silica nanocomposites prepared by the coprecipitation method”, *J. Magn. Mater.*, **323** (2011) 897–902.
16. G. Shi, Y. Mao, G. Ren, L. Gong, Z. Zhi, “Synthesis and photolysis of $\text{NaYF}_4@\text{SiO}_2@\text{TiO}_2$ core-shell nanocomposites”, *Opt. Commun.*, **332** (2014) 219–222.
 17. L. Liu, S. Yue, Y. Zhang, R. Qin, L. Liu, D. Zhang, R. Sun, L. Chen, “One-pot reverse microemulsion synthesis of core-shell structured $\text{YVO}_4:\text{Eu}^{3+}@\text{SiO}_2$ nanocomposites”, *Opt. Mater.*, **39** (2015) 207–210.
 18. W. Widiyastuti, I. Maula, S. Machmudah, T. Nurtono, S. Winardi, K. Okuyama, “Photocatalytic activity inhibition by ZnO-SiO_2 nanocomposites synthesized by sonochemical method”, *Adv. Mater. Res.*, **1112** (2015) 209–212.
 19. T.A. Hassan, V. Rangari, F. Baker, S. Jeelani, “Synthesis of hybrid SiC/SiO_2 nanoparticles and their polymer nanocomposites”, *Int. J. Nanosci.*, **12** (2013) 1350008.
 20. K.M.S. Khalil, H.A. Mahmoud, T.T. Ali, “Direct formation of thermally stabilized amorphous mesoporous $\text{Fe}_2\text{O}_3/\text{SiO}_2$ nanocomposites by hydrolysis of aqueous iron III nitrate in sols of spherical silica particles”, *Langmuir*, **24** (2008) 1037–1043.
 21. C. Chaneac, E. Tronc, J.P. Jolivet, “Magnetic iron oxide-silica nanocomposites. Synthesis and characterization”, *J. Mater. Chem.*, **6** (1996) 1905–1911.
 22. M. Zaharescu, M. Crisan, A. Jitianu, D. Crisan, A. Meghia, I. Rau, “ SiO_2 -iron oxide composites obtained by sol-gel method”, *J. Sol-Gel Sci. Technol.*, **19** (2000) 631–635.
 23. C. Cannas, G. Concas, F. Congiu, A. Musinu, G. Piccaluga, G. Z. Spano, “Mössbauer investigation of $\text{g-Fe}_2\text{O}_3$ nanocrystals in silica matrix prepared by the sol-gel method”, *Naturforsch.*, **57a** (2002) 154–158.
 24. M.V.J. Rocha, H.W.P. de Carvalho, V.H.V. Sarmiento, A.F. Craievich, T.C. Ramalho, “Structural characterization, thermal properties, and density functional theory studies of PMMA-maghemite hybrid material”, *Polym. Compos.*, **37** (2016) 51–60.
 25. F. Mammeri, E. Le Bourhis, L. Rozes, C. Sanchez, “Mechanical properties of hybrid organic-inorganic materials”, *J. Mater. Chem.*, **15** (2005) 3787–3811.
 26. K.-H. Haas, K. Rose, “Hybrid inorganic/organic polymers with nanoscale building blocks: precursors, processing, properties and applications”, *Rev. Adv. Mater. Sci.*, **5** (2003) 47–52.
 27. C. Sanchez, B. Julia, P. Belleville, M. Popall, “Applications of hybrid organic-inorganic nanocomposites”, *J. Mater. Chem.*, **15** (2005) 3559–3592.
 28. Y. Moriya, M. Sonoyama, F. Nishikawa, R. Hino, “Preparation of polymer hybrids of the porous materials made SiO_2 -PVA or SiO_2 -PEG system and from the hybrid gels”, *J. Ceram. Soc. Jpn.*, **101** (1993) 518–521.
 29. T. Yazawa, A. Miyake, H. Tanaka, “Preparation of porous SiO_2 - ZrO_2 glass from sol containing polyethylene glycol”, *J. Ceram. Soc. Jpn.*, **99** (1991) 1094–1097.
 30. K. Nakanishi, Y. Segawa, N. Soga, “Pore surface characteristics of macroporous silica gels prepared from polymer-containing solution”, *J. Non-Cryst. Solids*, **134** (1991) 39–46.
 31. S. Sato, T. Murakata, T. Suzuki, T. Ohgawara, “Control of pore size distribution of silica gel through sol-gel process using water soluble polymers as additives”, *J. Mater. Sci.*, **25** (1990) 4880–4885.
 32. G.J. Owens, R.K. Singh, F. Foroutan, M. Alqaysi, C.M. Han, C. Mahapatra, H.W. Kim, J.C. Knowles, “Sol-gel based materials for biomedical applications”, *Prog. Mater. Sci.*, **77** (2016) 1–79.
 33. R. Bryaskova, D. Pencheva, G.M. Kale, U. Lad, T. Kantardjiev, “Synthesis, characterisation and antibacterial activity of PVA/TEOS/Ag-Np hybrid thin films”, *J. Colloid. Interface Sci.*, **349** (2010) 77–85.
 34. P.S. Roy, J. Bagchi, S.K. Bhattacharya, “Size-controlled synthesis and characterization of polyvinyl alcohol coated palladium nanoparticles”, *Transition. Met. Chem.*, **34** (2009) 447–453.
 35. X. Qi, X. Yao, S. Deng, T. Zhou, Q. Fu, “Water-induced shape memory effect of graphene oxide reinforced polyvinyl alcohol nanocomposites”, *J. Mater. Chem. A*, **2** (2014) 2240–2249.
 36. M.R. Aguilar, J.S. Román, *Smart Polymers and their Applications*, 1st Edition, Elsevier, Woodhead Publishing, 2014.
 37. I. Jang, K. Song, S.G. Oh, “Synthesis of echinoid-like TiO_2 particles through modified sol-gel method using PVA as a surface-directing agent and their photocatalytic activity”, *Chem. Lett.*, **41** (2012) 173–174.
 38. S. Kralj, T. Potrč, P. Kocbek, S. Marchesan, D. Makovec, “Design and fabrication of magnetically responsive nanocarriers for drug delivery”, *Curr. Med. Chem.*, **23** (2016) 1–16.
 39. C. Ianăși., O.Costișor, A.M. Putz, J. Plocek, L. Săcărescu, D. Nižňanský, C. Savii, “Superparamagnetic $\gamma\text{-Fe}_2\text{O}_3\text{-SiO}_2$ nanocomposites from $\text{Fe}_2\text{O}_3\text{-SiO}_2$ -PVA hybrid xerogels. Characterization and MRI preliminary Ttesting”, in *Sustainable Organic And Hybrid Nanomaterials: From Structure To Functions*, special issue of Current Organic Chemistry, ed. M. Putz (accepted for publication).
 40. I. Mihalca, A. Ercuta, “Structural relaxation in $\text{Fe}_{70}\text{Cr}_{10.5}\text{P}_{11.5}\text{Mn}_{1.5}\text{C}_{6.5}$ amorphous alloy”, *J. Optoelectron. Adv. Mater.*, **5** (2003) 245–250.
 41. M. Raileanu, M. Crisan, C. Petrache, D. Crisan, M. Zaharescu, “ $\text{Fe}_2\text{O}_3\text{-SiO}_2$ nanocomposites obtained by different sol-gel routes”, *J. Optoelectron. Adv. Mater.*, **5** (2003) 693–698.
 42. A. Jitianu, M. Raileanu, M. Crisan, D. Predoi, M. Jitianu, L. Stanciu, M. Zaharescu, “ $\text{Fe}_3\text{O}_4\text{-SiO}_2$ nanocomposites obtained via alkoxide and colloidal route”, *J. Sol-Gel Sci. Technol.*, **40** (2006) 317–323.
 43. R.V. Kumar, Y. Koltypin, Y.S. Cohen, Y. Choen, D.

- Aurbach, O. Palchik, I. Felner, A. Gedanken, “Preparation of amorphous magnetite nanoparticles embedded in polyvinyl alcohol using ultrasound radiation”, *J. Mater. Chem.*, **10** (2000) 1125–1129.
44. M. Popovici, M. Gich, D. Nižňanský, A. Roig, C. Savii, L. Casas, E. Molins, K. Zaveta, C. Enache, J. Sort, S. de Brion, G. Chouteau, J. Nogués, “Optimized synthesis of the elusive ϵ -Fe₂O₃ phase via sol-gel chemistry”, *Chem. Mater.*, **16** (2004) 5542–5548.
 45. M. Hamdy, A. Ismail, “Thermoanalytic study of metal acetylacetonates”, *J. Anal. Appl. Pyrol.*, **21** (1991) 315–326.
 46. B. Pal, M. Sharon, “Preparation of iron oxide thin film by metal organic deposition from Fe(III)-acetylacetonate: a study of photocatalytic properties”, *Thin Solid Films*, **379** (2000) 83–88.
 47. C.J. Brinker, G.W. Scherer, *Sol-gel Science, The Physics and Chemistry of Sol-gel Processing*, Academic Press Inc., New York, 1990.
 48. T. Pirzada, S.A. Arvidson, C.D. Saquing, S.S. Shah, S.A. Khan, “Hybrid silica-PVA nanofibers via sol-gel electrospinning”, *Langmuir*, **28** (2012) 5834–5844.
 49. M. Stefanescu, M. Stoia, O. Stefanescu, C. Davidescu, G. Vlase, P. Sfirloaga, “Synthesis and characterization of poly(vinyl alcohol)/ethylene glycol/silica hybrids. Thermal analysis and FT-IR study”, *Rev. Roum. Chim.*, **55** (2010) 17–23.
 50. O. Karaagac, H. Kockar, “Effect of synthesis parameters on the properties of superparamagnetic iron oxide nanoparticles”, *J. Supercond. Nov. Magn.*, **25** (2012) 2777–2781.
 51. V.G. Tsirel’son, M.Y. Antipin, R.P. Strel’tsov, R.P. Ozerov, Y.T. Struchkov, “Electron density distribution and electric field gradient in hematite at 153 K determined from precision X-ray diffraction data”, *Dokl. Akad. Nauk. SSSR*, **298** (1988) 1137–1141.
 52. J.P. Dismukes, L.H. Jones, J.C. Bailar Jr., “The measurement of metal-ligand bond vibrations in acetylacetonate complexes”, *J. Phys. Chem.*, **65** [5] (1961) 792–795.
 53. K. Nakamoto, P. J. McCarthy, A. Ruby, A.E. Martell, “Infrared spectra of metal chelate compounds. II. Infrared spectra of acetylacetonates of trivalent metals”, *J. Am. Chem. Soc.*, **83** [5] (1961) 1066–1069.
 54. K. Kishi, S. Ikeda, K. Hirota, “Infrared and ultraviolet studies of the adsorption of acetylacetonate on evaporated iron and nickel films”, *J. Phys. Chem.*, **71** [13] (1967) 4384–4389.
 55. S. Musić, N. Filipović-Vinceković, L. Sekovanić, “Precipitation of amorphous SiO₂ particles and their properties”, *Braz. J. Chem. Eng.*, **28** [1] (2011) 89–94.
 56. V. Paredes-García, N. Toledo, J. Denardin, D. Venegas-Yazigi, C. Cruz, E. Spodine, Z. Luo, “One pot solvothermal synthesis of organic acid coated magnetic iron oxide nanoparticles”, *J. Chil. Chem. Soc.*, **58** [4] (2013) 2011–2015.
 57. K.S.W. Sing, “Reporting physisorption data for gas/solid systems with special reference to the determination of surface area and porosity”, *Pure. Appl. Chem.*, **54** (1982) 2201–2218.
 58. M. Thommes, “Physical adsorption characterization of nanoporous materials”, *Chemie. Ingenieur. Technik.*, **82** (2010) 1059–1073.
 59. S. Lowell, J.E. Shields, M.A. Thomas, M. Thommes, *Characterization of porous solids and powders: surface area, pore size and density*, Springer Science-Business Media, New York, 2004.

